N-body simulations in cosmology

Matej Blašković
Fizički odsjek, Prirodoslovno-matematički fakultet, Bijenička 32, Zagreb

Mentor: Cornelius Rampf
Institut Ruđer Bošković, Bijenička cesta 54, Zagreb

Abstract: N-body simulations are one of the key methods for modelling the large-scale structure of the universe, particularly structures such as galaxies, galaxy clusters, and dark matter halos, which exhibit highly nonlinear behavior that can be investigated through such simulations. This seminar will specifically examine how different parameterizations during the simulation setup affect the results. The emergence of errors due to the calculation of initial conditions and the discretization of mass in N-body systems is discussed. In that context, I analyze the impact of choosing an appropriate time for initializing the simulation, as well as explore various methods used to compute the mass density, which is a crucial bottleneck of any N-body method. Finally, the influence of mesh and particle resolution is also be studied. The goal is to obtain the most accurate simulation results possible, i.e., minimizing systematic errors.

I. INTRODUCTION

One of the most widely accepted theoretical models of the universe today proposes a universe dominated by dark energy, represented by a cosmological constant Λ, and dark matter making up the majority of matter. Dark matter, which appears to interact exclusively through gravity, is often modeled as a self-gravitating, pressureless (cold) fluid. These models are referred to as cold dark matter (CDM) models, and the corresponding cosmological model is called ΛCDM. In non-relativistic cases, the gravitational interaction of dark matter can be effectively described by Newtonian gravity, which becomes the dominant force on cosmological scales influencing the further evolution of the universe. As the universe evolves, highly nonlinear structures such as galaxies and galaxy clusters emerge, and the most accurate way to study such a universe becomes through numerical simulations. These simulations are a crucial method for testing the validity of potential cosmological models and identifying any flaws in the theoretical modelling. To achieve the highest precision, it is crucial to take into account well-established theoretical models that describe the behavior of dark matter in the universe, along with data derived from direct observations, such as fundamental constants. This approach allows for a more detailed description of the structure of dark matter, particularly on smaller scales where phenomena like dark matter halos are studied. Additionally, a variety of approximations are used when calculating initial conditions, gravitational potentials, or changes in the velocity and position of particles. The use of these methods must be carefully justified to ensure the most reliable information on mass distribution and the velocity field. Clearly, such simulations will involve numerous free parameters, which can significantly impact the final results. Specifically, N-body simulations are run with a large number of particles, and the goal is to make these simulations as accurate as possible in testing the theory. One of the obvious parameters that will affect the quality of the simulation is the simulation resolution of particle-mesh simulation, i.e., the number of particles and the number of grid points used to calculate the gravitational potential and force necessary to update the particle's momenta, Another important parameter is the choice of the initial conditions at the start of the simulation, i.e., the moment at which the initial conditions are calculated, as well as the order of perturbation theory used to calculate these conditions. The influence of all these parameters will be explored in this seminar. The remainder of this seminar is structured as follows. In Sec. II, the theoretical foundations necessary for understanding the calculation of initial conditions and the subsequent execution of the simulation are outlined. Sec. III focuses on the specifics of the simulation used in this study and presents the obtained results. In Sec. III A, the results of the individual simulation are discussed, while Sec. III B examines the impact of the choice of initial moment on the results. Sec. III C addresses the influence of methods for calculating mass density, and Sec. III D explores the effect of changes in resolution. Finally, Sec. IV presents the conclusions drawn from this study.

II. BASICS

To better understand these simulations, it is important to recognize that they consist of two main parts: first, the calculation of initial conditions that determine the initial deviations in the positions and velocities of particles from a completely uniform distribution, and second, the further propagation of particle motion driven by gravitational interaction. This section will provide a detailed explanation of how both components function within the simulation. In calculating the initial conditions, dark matter is modeled as an initially cold fluid, which is known to interact extremely weakly besides of gravity. For the purposes of the simulations, all interactions are described using Newtonian gravity. Then according to [1], the evolution of the dark-matter distribution, $f = f(\boldsymbol{x}, \boldsymbol{p}, t)$, is governed by the Vlasov–

Poisson equations (the collisionless Boltzmann-Poisson equations), which states that the total time derivative of f is conserved,

$$\frac{\partial f}{\partial t} + \frac{\boldsymbol{p}}{ma^2} \cdot \boldsymbol{\nabla}_{\boldsymbol{x}} f - m(\boldsymbol{\nabla}_{\boldsymbol{x}}\phi) \cdot \boldsymbol{\nabla}_{\boldsymbol{p}} f = 0\,, \tag{1}$$

$$\boldsymbol{\nabla}^2_{\boldsymbol{x}}\phi = 4\pi G\bar{\rho}(t)a^2(t)\,\delta(\boldsymbol{x},t)\,. \tag{2}$$

In (1), the first term explicitly depends on time, the second term describes the kinetic energy, and the third represents the gravitational interaction, where ϕ is the gravitational potential defined by (2), with the following parameters: G is the gravitational constant, $\bar{\rho}(t)$ is the average mass density of the universe at time t, $a = a(t)$ the scale factor of the universe defined by the Friedmann equation (see Eq. 4 below), and $\delta(\boldsymbol{x},t)$ is the deviation from the uniform density, as defined by the equation:

$$\rho = \bar{\rho}(1 + \delta(\boldsymbol{x},t))\,. \tag{3}$$

While the scale factor $a(t)$ is defined such that at the present time $a = 1$, and at the time of the big bang $a = 0$, through the Friedmann equation of the form in which K describes the uniform curvature, and Λ is the cosmological constant, crucial for current models that describe the accelerated expansion of the universe:

$$\left(\frac{\dot{a}}{a}\right)^2 = \frac{8\pi}{3}G\bar{\rho} - \frac{Kc^2}{a^2} + \frac{1}{3}\Lambda c^2\,. \tag{4}$$

Let us provide some qualitative considerations how dark matter evolves in time. Due to the topological nature of the distribution f in phase space, which occupies a 3-dimensional hypersurface in the full 6-dimensional phase space over time, this surface can be conceptualized as a thin sheet. Given the Hamiltonian nature of the system, this sheet remains continuous as it evolves. An important phenomenon in the evolution of such a phase space, driven by the gravitational attraction, is the folding of this thin sheet, a process known as shell-crossing (shown in Fig. 1 at 'time' $\tau = 1$ for a simplified one-dimensional setup). At this stage, infinite mass densities arise at specific points in space, and after the shell-crossing event, the cold dark matter fluid within the same region may exhibit multiple streams at some region of space. It is often emphasized that this initial shell-crossing is first shell-crossing, as further occurrences of shell-crossing are expected during the subsequent evolution. As discussed in [1], the formation of infinite densities and multistreams prevents exact analytical solutions and significantly complicates the application of approximation methods.

For solving the Vlasov–Poisson system and to facilitate tracking the evolution of the three-dimensional hypersurface, Lagrangian mapping is introduced using Lagrangian coordinates, commonly denoted as $\boldsymbol{q}$, which can be interpreted as a continuous set of particle labels. More details about the advantages of using the Lagrangian description of fluid flow can be found in [2]. Thus, if we assume a Lagrangian map of the form $\boldsymbol{q} \mapsto \boldsymbol{x}(\boldsymbol{q},t) = \boldsymbol{q} + \boldsymbol{\psi}(\boldsymbol{q},t)$,

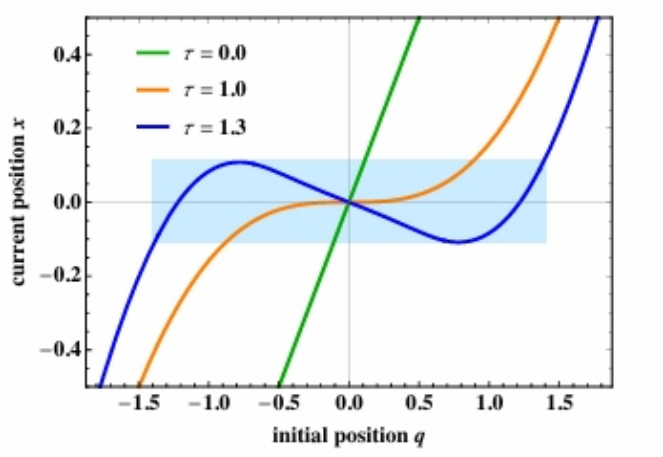

FIG. 1. Dependence of the Eulerian coordinate x on the Lagrangian coordinate q for the 1D case at the initial time ($\tau = 0$), at the time of shell-crossing ($\tau = 1$), and after shell-crossing ($\tau = 1.3$) calculated in [1]. The shaded region indicates the area where multistreams emerge.

where the Lagrangian map traces the path from the initial position q to the current Eulerian position x at time t, and where $\boldsymbol{\psi}$ is referred to as the Lagrangian displacement field. Figure 1 shows a nice representation of the dependence of the Eulerian position on the initial position at different time instances. The velocity field can then be easily represented as: $\boldsymbol{v} \equiv \dot{\mathbf{x}} = \dot{\boldsymbol{\psi}}$, where the overdot denotes the Lagrangian (total) time derivvative. In order for the Vlasov-Poisson equations to be regular at the initial time, we require boundary conditions, which can be seen in [1]: $\delta_{ini} = 0$ and $\boldsymbol{v}_{ini} = \dot{\boldsymbol{x}}(\boldsymbol{q}, t = 0)$ derived from the initial gravitational potential ϕ_{ini}. Furthermore, as shown in e.g. [3], the displacement field can be expanded in a series in $D_+ = D_+(t)$, which results in the following development:

$$\boldsymbol{\psi}(\boldsymbol{q},t) = \sum_{n=1}^{\infty} \boldsymbol{\psi}^{(n)}(\boldsymbol{q}) D_+^n\,. \tag{5}$$

Here, $D_+ = D_+(t)$ denotes the fastest growing mode solution in ΛCDM which can be represented by the Gauss hypergeometric function. Importantly, as shown in [4], the series representation (5) converges towards the exact solution before shell-crossing. Depending on the number of terms included in the expansion, we obtain a truncated solution of the initial conditions in the n-th order of Lagrangian perturbation theory ("nLPT"). Specifically, by taking only the first term, we obtain the 1LPT, known as the Zel'dovich approximation due to its significant contributions to cosmology. As expected, since we consider only a single term, this approximation is the simplest, and in certain specific, simple cases, exact analytical solutions can be obtained. Otherwise, it provides more intuitive and easily interpretable results, which can aid in the conceptual understanding of the early universe's evolution. Naturally, expanding the series to higher-order

terms yields more accurate results; however, it should be noted that each subsequent term becomes increasingly complex to calculate, making the computation of approximations like 2LPT or 3LPT more cumbersome numerically. A more detailed description of the calculation $\boldsymbol{\psi}$ up to 3LPT, as well as the calculation of ϕ_{ini}, which remains the only degree of freedom for the solution, can be found in [3]. It is also important to note the occurrence of aliasing due to the presence of quadratic terms and other nonlinearities in higher-order terms such as 2LPT and beyond which leads to non-linear modes appearing at the wrong wave numbers, thus causing errors. The emergence of aliasing increases the inaccuracy of the solution, and it can be avoided by using Orszag's 3/2 rule, as explained in [3]. Finally, the obtained solution is adjusted to a homogeneous and isotropic distribution of discrete particles, typically arranged in a simple cubic (SC) lattice. By displacing the positions and velocities of particles from the homogeneous lattice, which are calculated from $\boldsymbol{\psi}$, we obtain the initial conditions to initiate the next part of the simulation.

For the next part of the simulation, an important aspect is the integration of the Hamiltonian dynamics of the system, which will govern the trajectories of discrete particles in N-body simulations and describe the further evolution of the system. In such simulations, symplectic time integrators are often used, which enable the numerical updating of particle positions and velocities at specific time intervals. A good example of such integrators are leapfrog integrators, whose advantages can be found in [5, 6]. For these integrators, it is crucial that the update of particle positions and velocities occurs at different interleaved time steps. One example of such a leapfrog scheme is the drift-kick-drift (DKD) scheme described in [6], where, starting from initial positions $\boldsymbol{x}_n$ and velocities $\boldsymbol{v}_n$, in the first step we compute $\boldsymbol{x}_{n+1/2}$ as function of $\boldsymbol{x}_n$ and $\boldsymbol{v}_n$: $\boldsymbol{x}_{n+1/2} = f(\boldsymbol{x}_n, \boldsymbol{v}_n)$, in the second step $\boldsymbol{v}_{n+1} = f(\boldsymbol{x}_{n+1/2}, \boldsymbol{v}_n)$, and in the third step $x_{n+1} = f(\boldsymbol{x}_{n+1/2}, \boldsymbol{v}_{n+1})$, in order to obtain the values of x_{n+1} and v_{n+1} at the next time step, $n+1$, from the nth time step.By repeatedly applying such time steps, we evolve the system from an initial state defined by the initial conditions to the desired final state at a later stage in the system's evolution. In this context, position update operations are trivial and are referred to as drifts, whereas velocity update operations involve the calculation of the force as a function of position associated to the Poisson equation, making them considerably more complex, and are referred to as kicks. Since simulations often involve a vast number of particles, it would be impractical to calculate the interaction of each particle with all others. Therefore, an important aspect of force calculation is the approximation of the density distribution in space, from which the force is derived using Poisson's equation. One approach to solving this problem is outlined in [5]. This method involves setting up a stationary grid and computing the gravitational potential at the grid vertices. Then, Poisson's equation is solved in Fourier space using Fast Fourier Transforms (FFT). To enable this solution, it is not necessary to know the potential values at the grid vertices, because force calculation can be obtained by combining the following equations from the density distribution:

$$\boldsymbol{A}(\boldsymbol{x}) = -\boldsymbol{\nabla}_x \phi, \quad \boldsymbol{\nabla}^2_{\boldsymbol{x}} \phi = \delta(\boldsymbol{x})\,. \tag{6}$$

$\boldsymbol{A}$ is directly related to the force, and consequently, dictates the acceleration of the particles. For this, it will be necessary to assign the particle masses, for which there are no relevant discrete conditions for their positions, to the grid vertices in such a way that they most accurately represent the gravitational potential that governs their motion. Such assignments are referred to as mass assignment schemes. The simplest such scheme is the nearest grid point (NGP) scheme, which assigns the entire mass of a particle to the nearest grid point. A more refined scheme is the cloud-in-cell (CIC) method, where the mass assigned to a grid point is described by a continuous non differentiable function. In [5], the triangular-shaped cloud (TSC) scheme and the piecewise cubic spline (PCS) scheme are also described, where the mass assigned to a grid point is represented by a continuously differentiable function and a twice-continuously differentiable function, respectively. The 1D visualizations of these schemes can be seen in Figure 2.

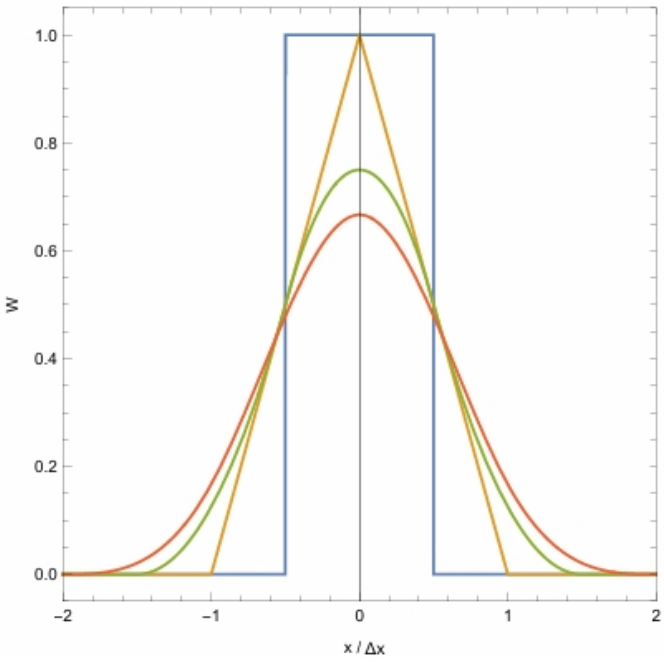

FIG. 2. dependence of the mass fraction assigned to the grid point w, on the particle's distance from the grid point x, in relation to the cell dimension Δx for the 1D case of mass assignment schemes from [5]. The schemes are color-coded as follows: NGP in blue, CIC in yellow,TSC in green, and PCS in orange.

It is evident that during the simulation process, numerous approximations are used, and it is expected that

systematic errors will arise when obtaining the results. Since this part of the simulation attempts to describe the evolution of the universe through a large number of discrete particles interacting gravitationally, these errors are a consequence of the discretization and are referred to as discretization errors. The most straightforward way to mitigate such errors would be to increase the simulation resolution, i.e., by increasing the number of particles and grid points. However, since running simulations with higher resolution demands greater computational power, reducing errors in this way is limited by the characteristics of the computing hardware. Another method for influencing errors would be to modify the mass assignment scheme, where we can study the impact of different parameterizations of mass assignment on the simulation results.

Additionally, considering the existence of errors arising from the calculation of initial conditions as well as discretization errors, an important parameter that will affect both types of errors is the choice of the moment at which the initial conditions are computed and the simulation is initiated. This moment is often determined by the starting redshift, which is defined in terms of the scale factor by the relation:

$$z = \frac{1}{a(t)} - 1\,. \tag{7}$$

Thus, the larger the redshift z, the earlier it corresponds to moments in the evolution of the universe, while $z = 0$ corresponds to the present time. Since the initial conditions are computed via the expansion (5), where we have the factor $D_+^n(t)$, it is clear that in the early epochs, the dominant contribution will come from the $n = 1$ term, while higher-order terms can be neglected. However, if we wish to track the evolution of the displacement field $\boldsymbol{\psi}$ over time, in later epochs, the contributions from higher-order terms will become more significant. Therefore, to minimize truncation errors arising from the initial conditions, it is advisable to include as many terms as possible in the expansion and to choose a higher starting redshift, i.e., an earlier initial moment. On the other hand, to reduce discretization errors, it is preferable to choose a smaller starting redshift [3]. This can be explained by the fact that as structures collapse into halos, the influence of initial conditions becomes less significant for the final result of the simulation, meaning that the errors in the simulation execution will be smaller as the universe's structure becomes more nonlinear. This behavior contrasts with the calculation of the initial conditions, which will be more accurate for a more linear structure of the universe. Clearly, it will be necessary to find a starting redshift z that balances both effects and minimizes both sources of error.

III. ANALYSIS OF SIMULATION RESULTS

For the execution of the simulations from which the results were obtained, I used the `Pysco` code presented in [7]. The code is written in Python and allows for the simulation of various cosmological models. Specifically, in this seminar, the focus will be on investigating the impact of the starting redshift, mass assignment scheme, and resolution on the final results, while other parameters remain unchanged during the simulations, with default values set within the code. These parameters include the use of Newtonian gravity and current values of cosmological constants: the Hubble constant $H_0 = 72$km/s/Mpc, matter density parameter $\Omega_{m0} = 0.25733$, which describes the today's mean matter content percentage wise in the universe assuming all matter behaves as dark matter while the rest of the universe energy budget is encoded in Λ, the temperature of the cosmic microwave background (CMB) in Kelvin, $T_{CMB} = 2.726$, effective number of neutrino species $N_{eff} = 3.044$, and the equation of state for dark energy $w_0 = -1.0$. The simulation box length was set to 100 Mpc/h, where h is the reduced Hubble constant, and the same random seed was used for initial conditions in all simulations. A symplectic leapfrog integrator with a kick-drift-kick (KDK) scheme was employed for time integration, while the time stepping and solver parameters were those recommended within the code. The parameters controlled within the code include the starting and ending redshifts, the number of particles and grid cells, the order of LPT used for calculating initial conditions, with options for 1LPT, 2LPT, and 3LPT, as well as the option for dealiased initial conditions. Additionally, the choice of mass assignment scheme between CIC and TSC was available. In the following sections, these parameters for each described simulation will be specified.

A. Results of a single simulation

During the simulation, special focus will be placed on two types of results. The first type consists of thin xy-slices at the final simulation time. These slices are obtained by utilizing the output from the code, which provides the x, y, and z components of the positions and velocities of all particles at a selected moment in the simulation. To visualize the final particle positions in a 2D representation, only those particles within a very narrow range of values for the z-coordinate are selected. Subsequently, it is advisable to use one of the mass assignment schemes, extracted from the code, in order to obtain a proper visualization of the mass density distribution on the 2D figure. Such an xy-slice is shown in Figure 3, where the TSC scheme is applied for the final image rendering at final redshift $z = 0$. This type of visualization provides a clear depiction of the large-scale structure of the universe, in which the structure of dark matter can

be observed, along with numerous high-density regions where dark matter gravitationaly collapses into halos and clusters.

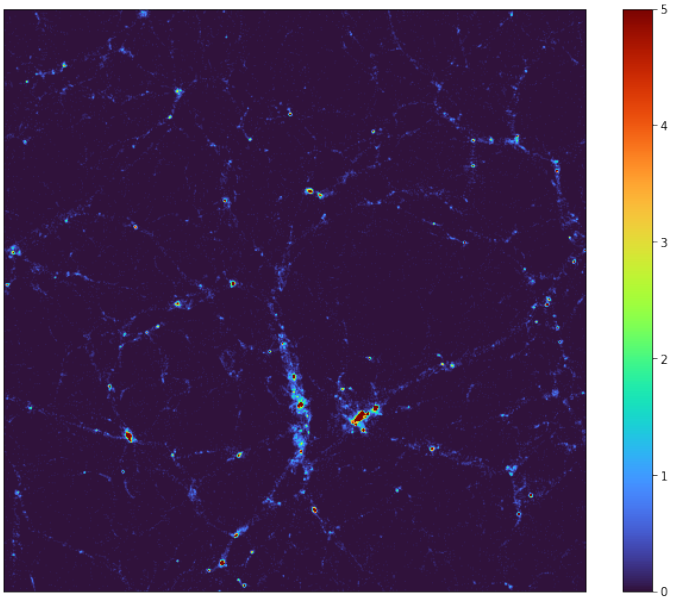

FIG. 3. xy-slice of the simulation performed with 512^3 particles and 512^3 grid points, starting at a redshift of $z = 49$, using 2LPT initial conditions and the TSC mass assignment scheme.

The second type of result to be analyzed is the matter power spectrum, for which the simulation provides output values of $P(k)$ for different k values at various redshifts throughout the simulation. The matter power spectrum is an important tool for analyzing the distribution of mass on cosmological scales. It represents a two-point statistic and is derived as the Fourier transform of the mass density autocorrelation function. As such, it describes fluctuations in the mass distribution across various scales in the universe, characterized by the wave number k. The lowest values of k for which the matter power spectrum is computed are limited by the box length in the simulation. However, since the primary aim of such simulations is to analyze smaller cosmological structures, which are characterized by highly nonlinear behavior, the study of the power spectrum values $P(k)$ for higher k becomes more relevant. It is also important to consider that the simulation has a finite resolution, which is constrained by the number of particles and grid points. In this context, the particle Nyquist wave number, denoted as $k_{Ny} = \frac{\pi N_p^{1/3}}{L_{box}}$, is commonly used. This represents the frequency of modes for which the average distance between two particles corresponds to half the wavelength of a sine wave. Consequently, we expect that discretization errors will become increasingly significant as the matter power spectrum approaches values near the Nyquist wave number. For values beyond this threshold, the results can no longer be considered reliable.

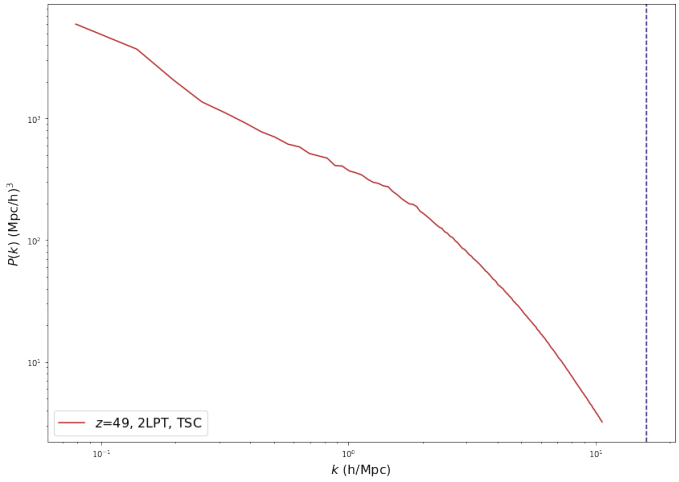

FIG. 4. Matter power spectrum of the same simulation as shown in Figure 3.

The matter power spectrum at the final redshift $z = 0$, obtained from the same simulation as the previous xy-slice, is shown in Figure 4, where the vertical line indicates the Nyquist wave number. This characteristic behavior of the power spectrum, which decreases with increasing k, is typical for N-body simulations, as demonstrated in [5]. In the following sections of the seminar, the focus will be on the differences in power spectra depending on the simulation parametrization. Additionally, the influence of the particle-to-gridpoint ratio on the power spectrum values near the Nyquist wave number will be discussed. It is also worth noting that this simulation, with 512^3 particles and grid points, is the most computationally demanding one that my system was able to run, requiring approximately one hour to complete. In contrast, the other simulations discussed later in the seminar are less demanding, primarily for practical reasons.

B. Impact of changes in the starting redshift

The first aspect to be investigated will be the effect of varying the initial redshift z on the final results for setting up 1LPT and 2LPT initial conditions. All simulations in this section were performed with 512^3 particles and 128^3 grid points, using the TSC mass assignment scheme and without employing dealiased initial conditions. Figure 5 shows the differences in the final xy-slices compared to the case with an initial redshift $z = 49$ and 2LPT initial conditions. The differences are presented both as the direct density difference and as the difference of the logarithms of the densities. As expected, these differences are most significant in regions where the matter density is higher, as we can observe that even by examining such a difference image, a clear sense of the large-scale mesh-like structure of the universe can be obtained.

The difference of the logarithms is shown to emphasize the presence of significant variations in low-density regions, and is expressed as $\ln(w_1+1)-\ln(w_2+1)$ where w_i are the computed particle number values at each grid point, obtained using mass assignment schemes from the code, proportional to the density. Considering that the scales are normalized to the same values, the differences are more pronounced at $z = 149$ compared to $z = 79$, which is expected since we assume that earlier initiation of the simulation has a stronger impact on the occurrence of discretization errors. On the other hand, 2LPT initial conditions should remain fairly accurate up to about the starting redshift $z = 30$, as demonstrated by the analysis in Figure 6.

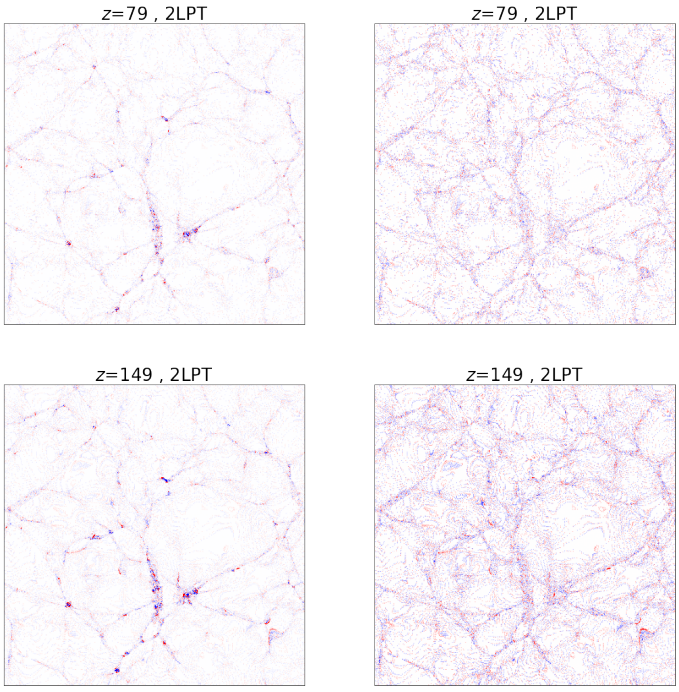

FIG. 5. Differences of the xy-slices for simulations with initial redshift $z = 79$ compared to $z = 49$, and $z = 149$ compared to $z = 49$, are shown, with the left panel displaying the density differences and the right panel showing the logarithmic density differences.

Figure 6 shows the ratios of the matter power spectra relative to the same benchmark as in the previous figure for various cases. First, let's analyze the spectra for the 1LPT case. It is evident that, within the range of initial redshifts between $z = 109$ and $z = 149$, the spectra are in good agreement. Deviations for redshifts above $z = 209$ can be attributed to the early initiation of the simulation, while deviations for lower redshifts, particularly below $z = 79$, can be explained by the need for more accurately defined initial conditions. For the 2LPT spectra, the differences are more pronounced, and it is observed that by shifting the starting redshift towards $z = 29$, the impact of discretization errors can be reduced. However, for even smaller starting redshifts, significant deviations arise primarily due to errors in the calculation of the initial conditions.

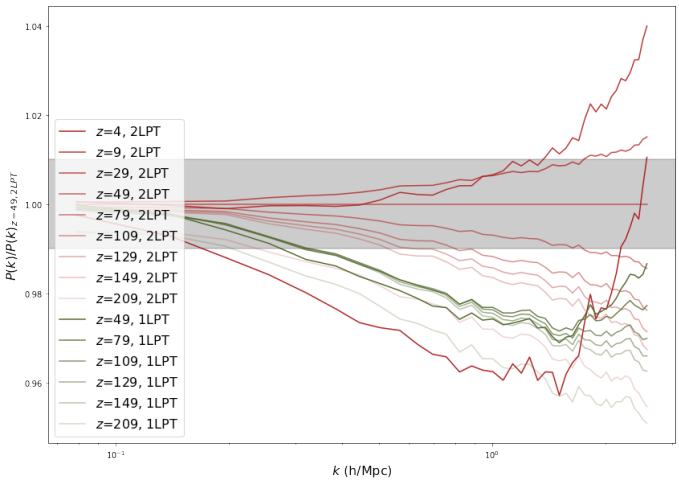

FIG. 6. matter power spectrum ratios relative to the 2LPT spectrum with a starting redshift $z = 49$ are shown.

C. Impact of changes in the mass assignament scheme

The second effect to be investigated is the impact of the mass assignment scheme on the simulation results. For all simulations, we use 512 particles, 128 grid points, 2LPT initial conditions, and a starting redshift $z = 49$. In the simulations shown in Figures 7 and 8, only the mass assignment schemes were modified for the entire simulation and for the calculation of the final xy-slice. In Figure 7, we observe the impact of different mass assignment schemes on the same xy-slice, with the differences being relatively small and most significant in regions of high mass density. In Figure 8, we see that even such a minor effect in the individual density calculations at grid points has a significant impact when the entire simulation is run using the same scheme. The most noticeable effects are again found in regions of high density, i.e., smaller cosmological structures. In Figure 9, we can see the matter power spectra for different mass assignment schemes and initial conditions at two different resolutions. It is evident that for sufficiently large k, the spectra obtained using the CIC scheme begin to deviate significantly from those obtained with the TSC scheme. These deviations can be mitigated by increasing the resolution, but they will still become significant for larger k. Since the TSC scheme is more accurate in describing the mass distribution, we can conclude that it is preferable to use it if we aim to more precisely determine the properties of universe structure on smaller scales.

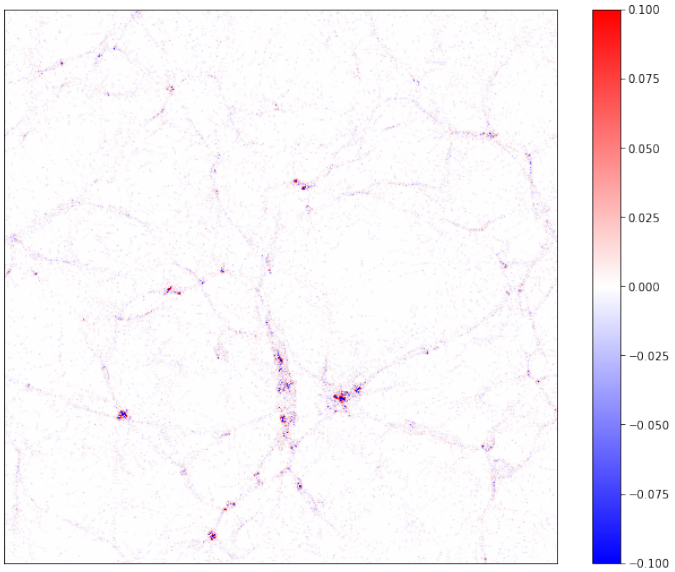

FIG. 7. The difference in the final xy-slices calculated using the TSC and CIC mass assignment schemes is shown for the case when the TSC scheme was used during the simulation run.

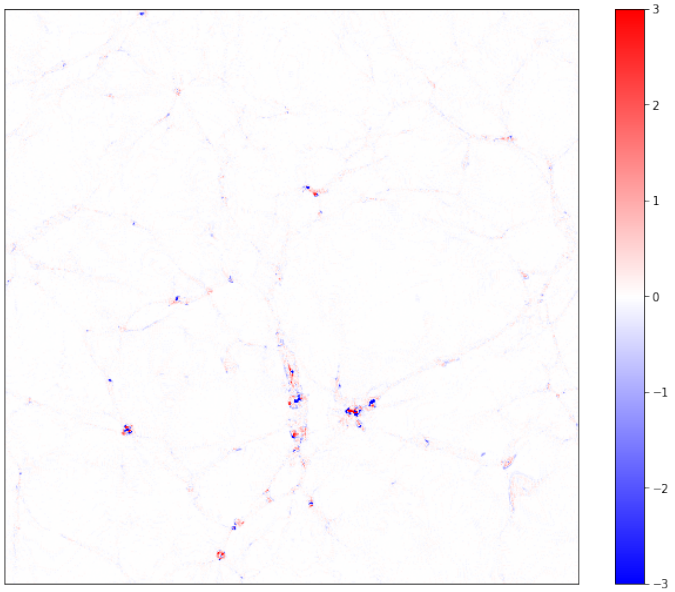

FIG. 8. The difference in the final xy-slices calculated using the TSC and CIC mass assignment schemes is shown for the case when the same schemes were used during the simulation run.

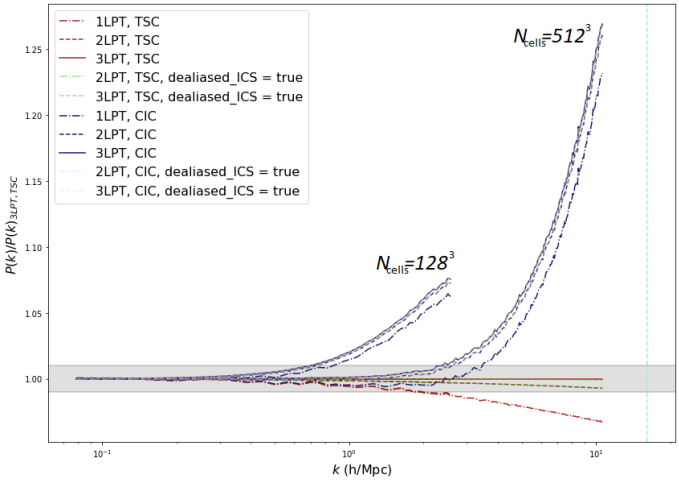

FIG. 9. matter power spectrum for simulations with starting $z = 49$ and 512^3 particles, using different initial conditions and grid point resolutions N_{cells}.

D. Impact of changes in the resolutins

Next, we will study the impact of resolution on the simulation results. In Figure 9, we present simulations run with various initial conditions and mass assignment schemes relative to the 3LPT, TSC case, using the same number of particles but different grid point resolutions. As expected, increasing the number of grid points improves the simulation resolution, resulting in more accurate solutions. First, we observe that by increasing the resolution, we can obtain values for the matter power spectrum $P(k)$ at higher k values, approaching closer to the Nyquist wave number. Furthermore, we note that enhancing the resolution significantly increases the precision of the simulation when using the CIC scheme, allowing for consistent results at higher wave numbers k. Finally, we observe that the effect of de-aliasing the initial conditions produces negligible corrections to the power spectra in this case. Since the TSC scheme has proven to be more accurate, the analysis for the last two figures will be conducted using only the TSC scheme. We will now examine the results of simulations with a lower number of particles than grid points for two initial redshift cases, 49 and 24, whose power spectra are shown in Figures 10 and 11. The first observation is that in this case, we can obtain values for $P(k)$ at k, which corresponds to the particle Nyquist wave number k_{Ny}. Furthermore, we observe the effect of de-aliasing corrections on the power spectrum near k_{Ny}, as predicted in [3]. That is, to obtain the most accurate results near k_{Ny}, it is necessary to set the resolution such that the number of particles is smaller than the number of grid points, and it is also beneficial to use dealiased initial conditions. Finally, by comparing Figures 10 and 11, we can observe the importance of using higher-order LPT if the simulation is to be started at later times, which is clearly seen in the significantly larger deviations for the 1LPT and 2LPT initial conditions at $z = 24$ compared to $z = 49$.

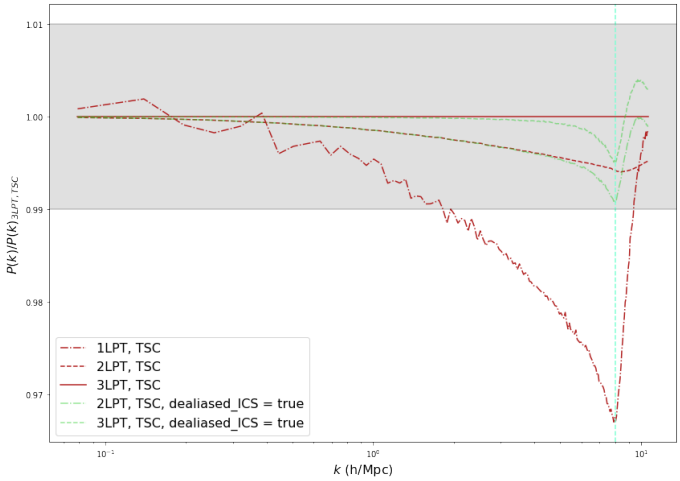

FIG. 10. matter power spectra with a resolution of 256^3 particles and 512^3 grid points, starting from $z = 49$ and ending at $z = 24$.

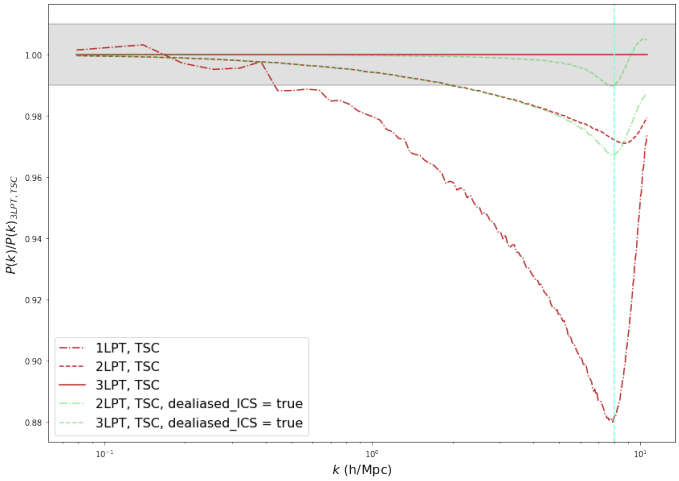

FIG. 11. Figure 11. matter power spectra with a resolution of 256^3 particles and 512^3 grid points, starting from $z = 24$ and ending at $z = 11.5$.

IV. CONCLUSIONS

In this seminar, the results obtained from various parameterizations during the execution of an N-body simulation are presented, focusing on their impact on the outcomes using the `Pysco` code. It is demonstrated that it is preferable to start the simulation at a later initial time (equivalent with choosing a small initial redshift), in order to reduce the impact of errors caused by particle discretization. However, for this it is crucial to employ a higher order approximation based on Lagrangian perturbation theory to minimize errors in the calculation of initial particle displacements and momenta, otherwise the simulation is affected by perturbative truncation errors. Additionally, we analyzed the impact of different mass assignment schemes on the simulation. It was observed that for sufficiently high wave numbers k, the values in the matter power spectrum $P(k)$ begin to diverge. Based on these findings, we conclude that for more accurate simulation results, particularly on small scales, the TSC scheme is preferred over the CIC scheme since it is more accurate. Finally, the impact of spatial resolution on the simulation results was examined. It was demonstrated that the most efficient way to utilize computational power in order to obtain optimal results at scales approaching the Nyquist wave number k_{Ny} is to ensure that the number of particles is slightly lower than the number of grid points. Additionally, the importance of using dealiased initial conditions was highlighted when approaching the wave number k_{Ny} for achieving higher precision in the results.

[1] C. Rampf, Cosmological Vlasov–Poisson equations for dark matter: Recent developments and connections to selected plasma problems, Rev. Mod. Plasma Phys. **5**, 10 (2021), arXiv:2110.06265 [astro-ph.CO].

[2] V. Zheligovsky and U. Frisch, Time-analyticity of Lagrangian particle trajectories in ideal fluid flow, J. Fluid Mech. **749**, 404 (2014), arXiv:1312.6320 [math.AP].

[3] M. Michaux, O. Hahn, C. Rampf, and R. E. Angulo, Accurate initial conditions for cosmological N-body simulations: Minimizing truncation and discreteness errors, **500**, 663 (2020), arXiv:2008.09588 [astro-ph.CO].

[4] C. Rampf and O. Hahn, Shell-crossing in a ΛCDM Universe, **501**, L71 (2021), arXiv:2010.12584 [astro-ph.CO].

[5] R. E. Angulo and O. Hahn, Large-scale dark matter simulations, Liv. Rev. Comput. Astrophysics **8**, 1 (2022), arXiv:2112.05165 [astro-ph.CO].

[6] C. Rampf, F. List, and O. Hahn, BullFrog: Multi-step perturbation theory as a time integrator for cosmological simulations, (2024), arXiv:2409.19049 [astro-ph.CO].

[7] M.-A. Breton, PySCo: A fast Particle-Mesh N-body code for modified gravity simulations in Python, (2024), arXiv:2410.20501 [astro-ph.CO].